Sensors and Materials, Vol. 33, No. 12 (2021) 4265–4281
MYU Tokyo

S & M 2760

Implementation and Optimization of Two Degree of Freedom H_∞ Loop Shaping Control for Average Current Mode Control Buck Converter using Genetic Algorithm

Somyot Kaitwanidvilai,[1] Nuttapon Phurahong,[2] and Warachart Suwan-ngam[1*]

[1]School of Engineering, King Mongkut's Institute of Technology Ladkrabang,
1 Soi Chalongkrung 1 Ladkrabang, Bangkok 10520, Thailand
[2]Phetchabun Rajabhat University, 83 Moo 11 Muang District, Phetchabun 67000, Thailand

(Received March 20, 2021; accepted November 16, 2021)

Keywords: 2DOF H_∞ loop shaping control, implementation, genetic algorithm, ACMC buck converter

In this paper, we focus on the implementation and optimization of two degree of freedom (2DOF) H_∞ loop shaping control for the DC-DC buck converter. The output voltage is controlled using the current control mode called the average current mode control (ACMC). The technique using the fixed structure robust controller technique, as well as genetic algorithm (GA), is applied, resulting in the reduction of the controller order and optimal parameter for the robust proportional integral (PI) controller. In this paper, the performance of the proposed controller is compared with those using the conventional 2DOF H_∞ loop shaping controller and other techniques. According to both simulation and experimental results, the robust controller designed by the proposed technique is simple, low order, and practical, yet still retains both performance and robustness.

1. Introduction

A DC-DC buck converter has been widely used in several applications such as electrical applications from low to high voltage but with a low power rating owing to its simplicity. The output voltage of the buck converter is lower than its input voltage. The required output voltage can be achieved by controlling the duty cycle of the controllable switch. In such circuit, the LC low-pass filter is used to remove the high-frequency component of the output voltage. Robustness and high performance are required to support different types of load and to tolerate any disturbance. Several control techniques that can synthesize the robust controller, such as the conventional H_∞ loop shaping control and 2DOF H_∞ loop shaping control with H_2/H_∞ mixed sensitivity,[1–4] have been applied to control the output voltage of the buck converter. However, such techniques result in high-order robust controller structures causing impracticability of implementation in real systems. The fixed structure robust loop shaping control using genetic algorithm (GA) described in Refs. 5 and 6 already solved this problem while retaining the high performance and robustness. However, it does not support the time domain response. Therefore, in a previous work,[7] the proposed technique called fixed structure robust 2DOF H_∞ loop shaping control using GA solved all these problems.

*Corresponding author: e-mail: warachart.su@kmitl.ac.th
https://doi.org/10.18494/SAM.2021.3368
(Revised: December 24, 2021)

ISSN 0914-4935 © MYU K.K.
https://myukk.org/

In this paper, we focus on the implementation of the controllers, which are synthesized by the proposed technique, to the buck converter. This paper starts with the converter model describing the mode control of the DC-DC buck converter. In Sect. 3, we present the principle of 1DOF H_∞ loop shaping control, 2DOF H_∞ loop shaping control, and the proposed technique. The simulation and experimental results are presented and discussed in Sect. 4. Finally, the conclusion is given in Sect. 5.

2. Converter Model

There are two control modes for the DC-to-DC converter: voltage mode control (VMC) and current mode control (CMC).[8] VMC is simple and requires no current sensor. Only a single voltage loop is required, but the overcurrent protection is not quite effective. CMC is different. The cascaded control is applied and adopted: the voltage control loop followed by the inductor current control loop. The output of the voltage control loop becomes the reference for the inductor current control loop. Two current control modes are generally applied to the DC-DC buck converter: peak current mode control (PCMC) and average current mode control (ACMC).[9–13] However, PCMC suffers from noise and has low current loop gain. Conversely, ACMC does not have this problem owing to the existence of the compensator in the current loop. Therefore, ACMC is preferable and selected. The general circuit diagram of the analog current loop controller is depicted in Fig. 1. From Fig. 1 and Ref. 5, the transfer function of the inner current loop compensator can be written as shown in Eq. (1).

$$G_{CA}(s) = \frac{K_c\left(1+\dfrac{s}{\omega_z}\right)}{s\left(1+\dfrac{s}{\omega_p}\right)}, \tag{1}$$

where $K_c = 1/(R_l(C_{fp} + C_{fz}))$, $\omega_z = 1/R_fC_{fz}$, and $\omega_p = (C_{fz} + C_{fp}) / (R_fC_{fz}C_{fp})$ The parameter of the composition of such circuit can be calculated using Eq. (2).

$$\frac{R_f}{R_l} \le \min\left[\frac{2V_mLf_s}{V_{g,\max}R_s}, \frac{V_mLf_s}{V_oR_s}\right], \tag{2}$$

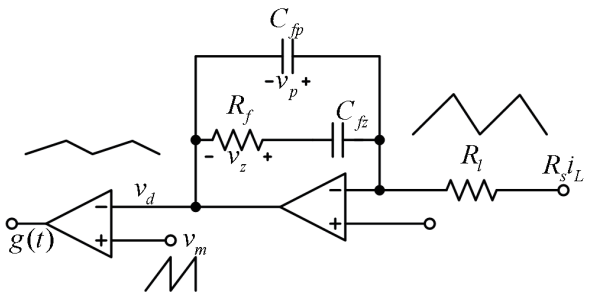

Fig. 1. Structure of inner current loop controller.

where V_m is the peak-to-peak voltage, R_s is the current sensing resistance, and V_g is the input voltage.

The control-to-output voltage transfer function[9–13] of the ACMC buck converter can be derived as shown in Eq. (3).

$$\frac{V_o(s)}{V_c(s)} = \frac{K_m(1+r_cCs)[G_{CA}+1]G_{dv}(s)}{1+T_c(s)}, \tag{3}$$

where K_m is the modulator gain ($K_m = 1/V_m$), r_c is the equivalent series resistor (ESR), G_{CA} is the transfer function of the current loop compensator, G_{dv} is the transfer function from the duty cycle to the output voltage, and T_c is the current loop gain. The circuit diagram of the ACMC buck converter is shown in Fig. 2. In this paper, the voltage controller is designed using the 2DOF H_∞ loop shaping control and the proposed technique.

3. Principles of 1DOF H_∞ Loop Shaping Control, 2DOF H_∞ Loop Shaping Control, and Proposed Technique

3.1 1DOF H_∞ Loop Shaping Control

The conventional H_∞ loop shaping control is an efficient technique that can be used to synthesize the robust controller, but this technique supports only the frequency domain. Two important parameters are required for shaping the nominal plant (G): pre-compensator weight function (W_1) and post-compensator weight function (W_2), as shown in Eq. (4). The shaped plant (G_s) is then separated into the normalized nominator factor (N_s) and denominator factor (M_s) as shown in Fig. 3, which is the uncertainty model of the plant.

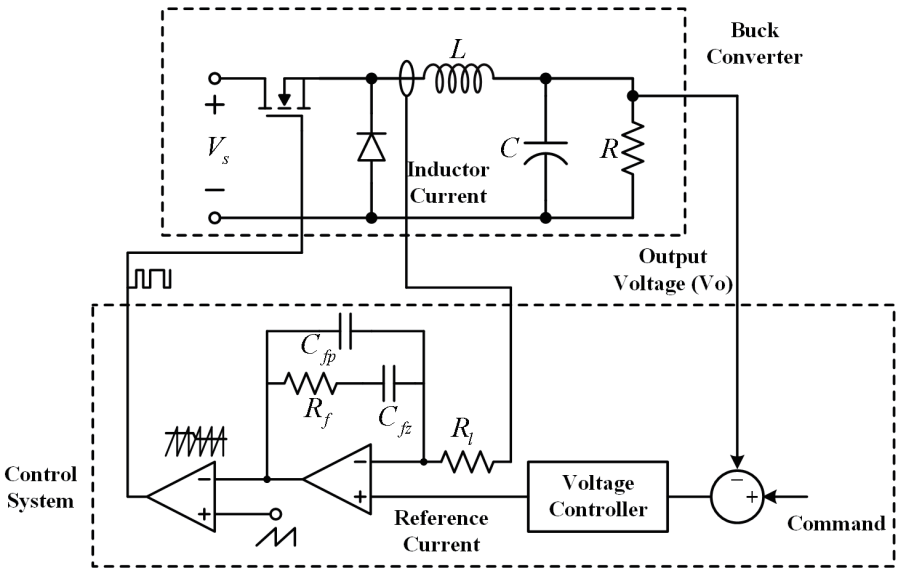

Fig. 2. Circuit diagram of ACMC buck converter.

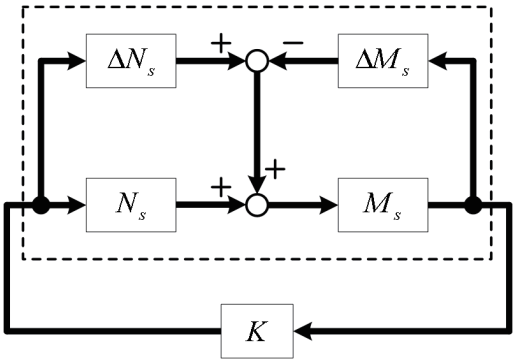

Fig. 3. 1DOF H_∞ robust stabilization problem.

The shape plant (G_s) and the perturbed plant (G_Δ) can be written as shown in the following Eqs. (4) and (5), respectively.

$$G_s = W_1 G W_2 = M_s^{-1} N_s \tag{4}$$

$$G_\Delta = (N_s + \Delta N_s)(M_s + \Delta M_s)^{-1} \tag{5}$$

From Eq. (4), by neglecting the noise of the sensor, W_2 can be the identity matrix. From Eq. (5), G_Δ is the shaped plant with uncertainty, whereas ΔN_s is the uncertainty transfer function in the nominator factor and ΔM_s is the uncertainty transfer function in the denominator factor. The stability margin of the plant (ε) can be calculated as

$$\|\Delta N_s, \Delta M_s\|_\infty \leq \varepsilon. \tag{6}$$

The perturbed feedback system shown in Fig. 3 is robust only when $\varepsilon > 0.25$; therefore, if this condition is not met, the weight function must be redesigned. The maximum stability margin can be calculated by solving the Riccati equation using Eq. (7).

$$\gamma_{\min} = \varepsilon_{\max}^{-1} = \left(1 + \lambda_{\max}(XZ)\right)^{\frac{1}{2}} \tag{7}$$

$$\left\| \begin{bmatrix} K_\infty \\ I \end{bmatrix} (I - G_s K_\infty)^{-1} M^{-1} \right\|_\infty \leq \varepsilon^{-1} \tag{8}$$

Equation (8) is also equivalent to Eq. (9).

$$\left\| \begin{matrix} K_\infty S & K_\infty S G_\infty \\ S & S G_\infty \end{matrix} \right\|_\infty \leq \varepsilon^{-1}, \tag{9}$$

where $S = (I - G_s K_\infty)^{-1}$.

Finally, the robust controller can be determined using Eq. (10).

$$K = W_1 K_\infty W_2 \tag{10}$$

3.2 2DOF H_∞ Loop Shaping Control

The desired response in both frequency domains may not be adequate in some applications. The 2DOF H_∞ loop shaping control technique can help solve this problem. Two controllers, namely, the pre-filter controller (K_1) and the feed-back controller (K_2), are the outcomes of this technique. The feed-back controller is responsible for the frequency domain response in relation to robustness and performance. The pre-filter controller is responsible for the time domain response in relation to the desired step response of the system in comparison with the reference model (T_{ref}). By this technique, shaping the plant requires only W_1. The perturbed plant can be calculated using the 1DOF H_∞ loop shaping control technique. The co-prime factor that separates the shaped plant into N_s and M_s is shown in Fig. 4. W_1 can be acquired from the synthesized stability margin value ε. If ε is less than 0.25, W_1 must be redesigned. Both K_1 and K_2 are synthesized by solving the problem in Fig. 5. From Fig. 5, ρ is a scalar value used for specifying the degree of significance in the time domain. T_{ref} is the desired closed-loop transfer function to specify the step response of a plant in the time domain by the designer, so the stability margin can be calculated using Eq. (11).

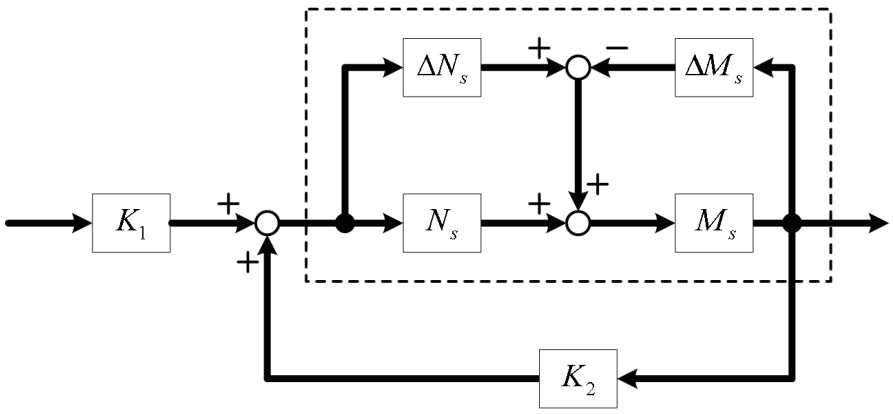

Fig. 4. 2DOF H_∞ robust stabilization problem.

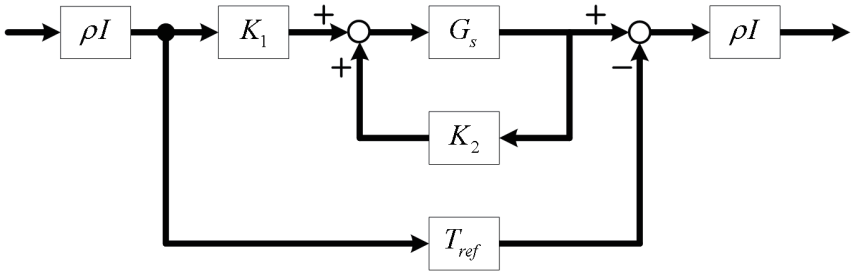

Fig. 5. 2DOF H_∞ loop shaping design problem.

$$\gamma\rho^{-2} = \varepsilon^{-1}\rho^{-2} = \left\|(I - G_s K_2)^{-1} G_s K_1 - T_{ref}\right\|_\infty \tag{11}$$

$K_{1\infty}$ and $K_{2\infty}$ can be synthesized by solving Eq. (12).

$$\left\|T_{wz}\right\|_\infty = \left\| \begin{bmatrix} \rho\left(I - G_s K_{2\infty}\right)^{-1} K_{1\infty} & K_{2\infty}\left(I - G_s K_{2\infty}\right)^{-1} M^{-1} \\ \rho\left(I - G_s K_{2\infty}\right)^{-1} G_s K_{1\infty} & \left(I - G_s K_{2\infty}\right)^{-1} M^{-1} \\ \rho^2\left[\left(I - G_s K_{2\infty}\right)^{-1} G_s K_{1\infty} - T_{ref}\right] & \rho\left(I - G_s K_{2\infty}\right)^{-1} M^{-1} \end{bmatrix} \right\|_\infty \le \varepsilon^{-1} \tag{12}$$

Finally, K_1 and K_2 can be determined from Eqs. (13) and (14), respectively.

$$K_1 = W_1 K_{1\infty} W_i \tag{13}$$

$$K_2 = W_1 K_{2\infty} \tag{14}$$

Here, W_i is a scalar value that is calculated using Eq. (15).

$$W_i = \left[W_o \left\{ I - G_s(0) K_{2\infty}(0) \right\}^{-1} G_s(0) K_{1\infty}(0) \right]^{-1} T_{ref}(0)\,, \tag{15}$$

where W_o is the identity matrix.

3.3 Proposed Technique

On the basis of the conventional 2DOF H_∞ loop shaping control, the proposed technique can be used to synthesize two robust controllers, namely, the feed-back controller (K_2) and the pre-filter controller (K_1), providing support to both frequency and time domains. K_2 can be synthesized by the fixed structure 1DOF H_∞ loop shaping control method to meet the desired robustness and performance. K_1 can be synthesized by the minimum integral of the square error (ISE) method to meet the desired time domain response. In this paper, the GA is applied to find the optimal parameters of K_1 and K_2. Both K_1 and K_2 are designed to have the 1st-order structure; therefore, the problem of high order arising from the conventional 2DOF H_∞ loop shaping control method is solved. The procedure for designing the robust controller using the proposed technique can be summarized as follows.

Step 1. Shape the nominal plant G using W_1. The transfer function of W_1 is shown in Eq. (16). Once the plant is shaped, we calculate ε_{opt} and check whether $\varepsilon_{opt} < 0.25$. If $\varepsilon_{opt} < 0.25$, we redesign the parameters of W_1.

$$W_1 = \frac{as + b}{s + 0.001} \tag{16}$$

Step 2. Design the transfer function of the feed-back controller $K_2(p_2)$ (p_2 is the parameter of K_2) using Eq. (17). $K_{2\infty}$ is used for synthesizing ε_{opt} as shown in Eq. (8). In this paper, K_2 is designed as a proportional integral (PI) controller as shown in Eq. (18).

$$K_{2\infty} = W_1^{-1} K_2(p_2) \tag{17}$$

$$K_2(p_2) = K_2 p + \frac{K_2 i}{s} \tag{18}$$

Step 3. Specify all the GA parameters[7,14] such as the size of the population in use, maximum generation, and probability of crossover and mutation for synthesizing the optimal stability margin (ε_{opt}).

Step 4. Synthesize ε_{opt} using the 1DOF H_∞ loop shaping control method. The minimum fitness function $(J_{\text{cost}})^{-1}$ is the value of ε_{opt} as shown in Eq. (19). We set the first generation as Gen1.

$$\begin{aligned} \left(J_{\text{cost}}\right)^{-1} &= \varepsilon_{opt} \\ &= \left(\left\| \begin{bmatrix} W_1^{-1} K_2(p_2) \\ I \end{bmatrix} (I - G_s W_1^{-1} K_2(p_2))^{-1} M^{-1} \right\|_\infty \right)^{-1} \end{aligned} \tag{19}$$

Step 5. Increase the generation for a step and go to step 4 to synthesize ε_{opt} of each generation until the current generation is the maximum generation.

Step 6. Check robustness and performance in the frequency domain. If robustness and performance are unsatisfactory, go to step 2 to redesign the parameters of K_2 or go to step 3 to change the boundary of the population size.

Step 7. Specify the transfer function of a pre-filter controller, $K_1(p_1)$ (p_1 is the parameter of K_1). The designed structure of K_1 in this paper is shown in Eq. (20).

$$K_1(p_1) = \frac{1}{K_1 s + 1} \tag{20}$$

Step 8. Specify T_{ref}, and then use GA to synthesize $K_1(p_1)$. Compare T_{ref} by evaluating the minimum ISE.[15]

4. Simulation and Experimental Results

The simulation was performed using the MATLAB/Simulink program to compare the performance of the proposed robust controller with those of the other controllers. The DC-DC buck converter that is controlled by the proposed controller has the parameters shown in Table 1.

Moreover, as shown in Fig. 2, the inner current loop controller is an analog controller. The parameters of such controllers are as follows: R_1 = 1 kΩ, R_f = 10 kΩ, C_{fz} = 27 nF, and

Table 1
Parameters of ACMC buck converter.

Parameter	Description	Value
V_g	Input voltage	24 V
V_o	Output voltage	10 V
R	Load	1.5 Ω
L	Inductor	100 µH
C	Capacitor	220 µF
f_{sw}	Switching frequency	10 kΩ

C_{fp} = 2.2 nF. In reference to Table 1 and Eq. (1), the transfer function of the plant in the voltage loop is shown in Eq. (21).

$$G = \frac{\left(\begin{array}{l} 3.168x10^{-17}s^5 + 1.936x10^{-11}s^4 + 9.979x10^{-7}s^3 \\ + 0.00643s^2 + 50.86s + 1.233x10^5 \end{array}\right)}{\left(\begin{array}{l} 4.356x10^{-25}s^7 + 5.143x10^{-20}s^6 + 4.606x10^{-15}s^5 + 1.854\,x10^{-10}s^{-4} \\ + 1.682x10^{-6}s^3 + 0.012s^2 + 48.02s + 6.164x10^4 \end{array}\right)} \tag{21}$$

From Eq. (16), with the parameters provided, W_1 and T_{ref} are designed as shown in Eqs. (22) and (23), respectively. The parameter ρ is set to 0.7.[6]

$$W_1 = \frac{1.5s + 9500}{s + 0.001} \tag{22}$$

$$T_{ref} = \frac{1}{0.18 \times 10^{-3}s + 1} \tag{23}$$

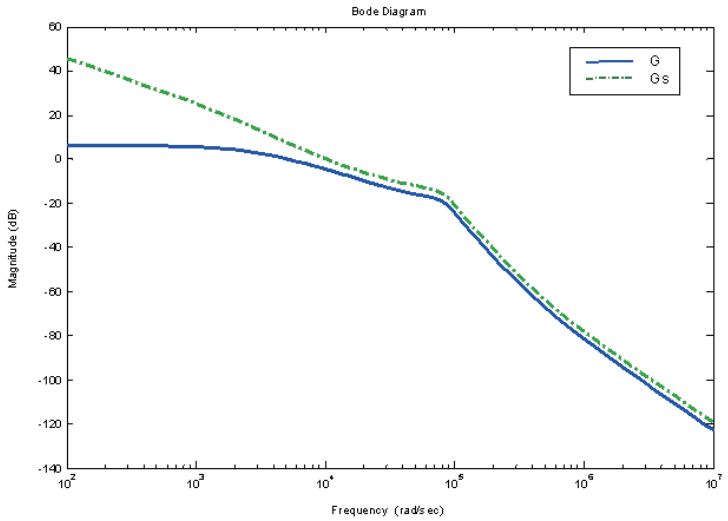

Fig. 6. (Color online) Bode plots of nominal plant G and shaped plant G_s.

Therefore, the shaped plant $G_s = W_1 G$ becomes Eq. (24).[6] ε_{max} is found as 0.626. The Bode plots of the nominal plant and the shaped plant are shown in Fig. 6.

$$G_s = \left(\frac{1.5s + 9500}{s + 0.001}\right) \times \frac{(3.168x10^{-17}s^5 + 1.936x10^{-11}s^4 + 9.979x10^{-7}s^3 + 0.00643s^2 + 50.86s + 1.233x10^5)}{(4.356x10^{-25}s^7 + 5.143x10^{-20}s^6 + 4.606x10^{-15}s^5 + 1.854\,x10^{-10}s^{-4} + 1.682x10^{-6}s^3 + 0.012s^2 + 48.02s + 6.164x10^4)} \tag{24}$$

Finally, with the conventional 2DOF H_∞ loop shaping control, the transfer functions of $K_1$and K_2 can be derived using Eqs. (25) and (26), respectively.[6] In this case, the stability margin ε is found to be 0.558 and W_i is 4.17.

$$K_1 = W_1 K_{1\infty} W_i = \frac{\left(\begin{array}{l} 2.326\times10^6 s^8 + 1.998\times10^{11}s^7 + 1.982\times10^{16}s^6 + 4.661\times10^{20}s^5 \\ + 5.474\times10^{24}s^4 + 4.118\times10^{28}s^3 + 2.104\times10^{32}s^2 + 6.358\times10^{35}s + 7.871\times10^{38} \end{array}\right)}{\left(\begin{array}{l} s^9 + 2.787\times10^6 s^8 + 2.77\times10^{11}s^7 + 2.574\times10^{16}s^6 + 4.158\times10^{20}s^5 \\ + 3.613\times10^{24}s^4 + 2.164\times10^{28}s^3 + 7.499\times10^{31}s^2 + 1.007\times10^{35}s + 1.007\times10^{32} \end{array}\right)} \tag{25}$$

$$K_2 = W_1 K_{2\infty} = \frac{\left(\begin{array}{l} -5.274\times10^6 s^8 - 4.273\times10^{11}s^7 - 4.244\times10^{16}s^6 - 8.622\times10^{20}s^5 \\ -9.038\times10^{24}s^4 - 6.314\times10^{28}s^3 - 2.915\times10^{32}s^2 - 7.537\times10^{35}s - 7.871\times10^{38} \end{array}\right)}{\left(\begin{array}{l} s^9 + 2.787\times10^6 s^8 + 2.77\times10^{11}s^7 + 2.574\times10^{16}s^6 + 4.158\times10^{20}s^5 \\ +3.613\times10^{24}s^4 + 2.164\times10^{28}s^3 + 7.499\times10^{31}s^2 + 1.007\times10^{35}s + 1.007\times10^{32} \end{array}\right)} \tag{26}$$

However, the orders of both K_1 and K_2 are 9th, which is very difficult to implement. The model order reduction should be performed. In this paper, the Hankel singular value technique is applied to reduce the model order as shown in Fig. 7, and the results are shown in Eqs. (27) and

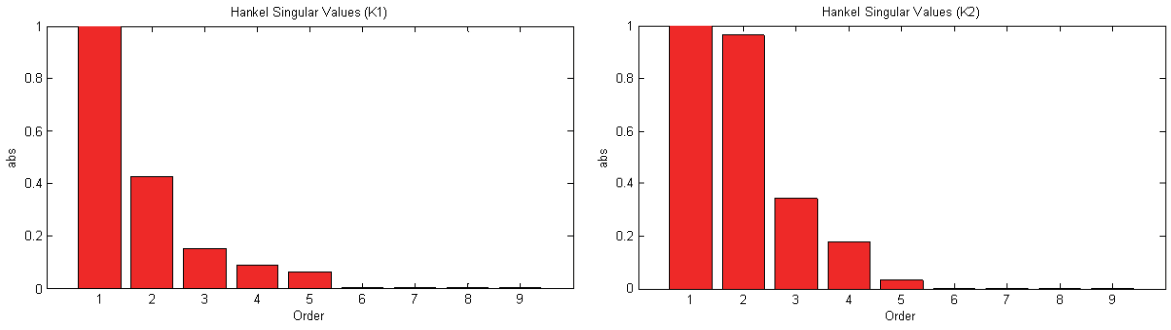

(a) (b)

Fig. 7. (Color online) Hankel singular value. (a) Pre-filter controller. (b) Feed-back controller.

(28), respectively. The results show that the reduced order of K_1 and K_2 is still high (5th order). Although the robustness and high performance are still retained, the structure is too complicated to implement in real systems.

$$K_1 = \frac{2.333\times10^6 s^4 + 1.713\times10^{11} s^3 + 1.769\times10^{16} s^2 + 2.324\times10^{20} s + 8.593\times10^{23}}{s^5 + 2.783\times10^6 s^4 + 2.423\times10^{11} s^3 + 2.277\times10^{16} s^2 + 1.1\times10^{20} s + 1.1\times10^{17}} \quad (27)$$

$$K_2 = \frac{-5.265\times10^6 s^4 - 3.519\times10^{11} s^3 - 3.664\times10^{16} s^2 - 2.937\times10^{20} s - 5.749\times10^{23}}{s^5 + 2.768\times10^6 s^4 + 2.375\times10^{11} s^3 + 2.192\times10^{16} s^2 + 7.357\times10^{19} s + 7.358\times10^{16}} \quad (28)$$

To overcome the complexity of implementing the conventional controller, the 1st-order filter and PI controller are synthesized using the proposed technique without losing robustness and performance. In this case, the GA runs for 150 generations for K_2, whereas it runs for 122 generations for $\varepsilon = 0.594$, as shown in Fig. 8. The synthesized transfer function of K_2 is shown in Eq. (29).

$$K_2(p_2) = 1.43 + \frac{7.72\times10^3}{s} \quad (29)$$

Considering the performance of the system using only K_2, the step response is shown in Fig. 9. Likewise, this controller is designed to be applied with the proposed technique as shown in Eq. (29).

As previously discussed, the feed-back controller is synthesized to support the frequency domain response. Considering the step response in the time domain, the 5.94% overshoot does not satisfy the time domain response. Moreover, the settling time achieved is 0.743 ms, whereas the rise time is 0161 ms. In this case, the stability margin is 0.594.

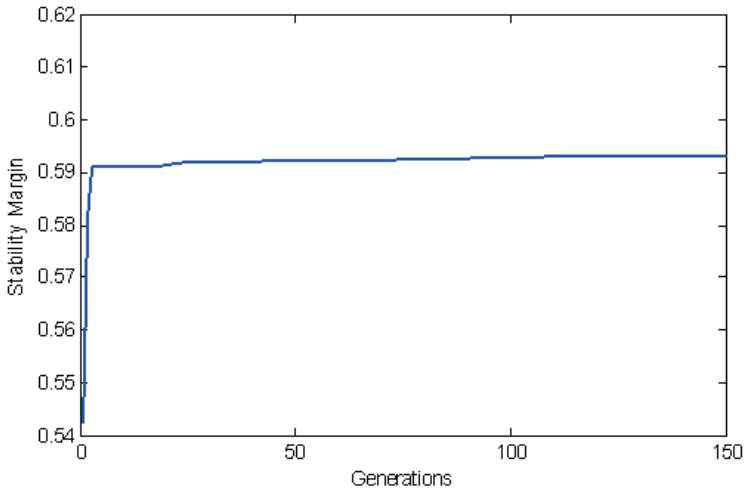

Fig. 8. (Color online) Stability margins of each generation.

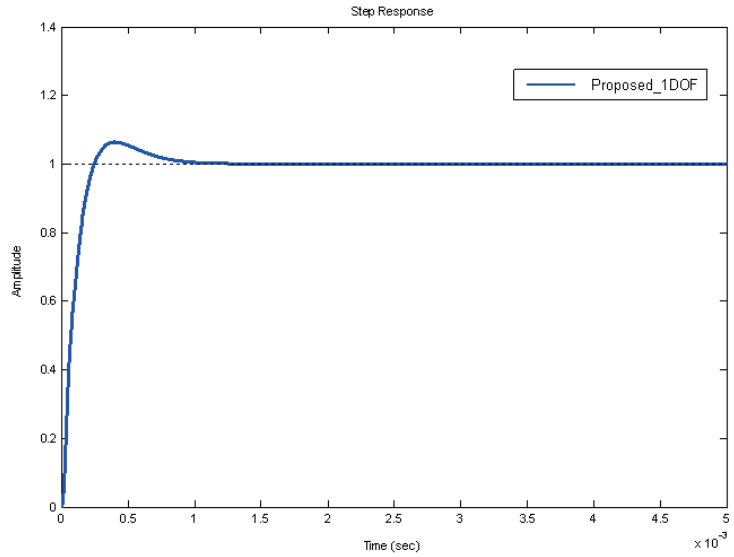

Fig. 9. (Color online) Step response of proposed technique by using 1DOF H_∞ loop shaping control.

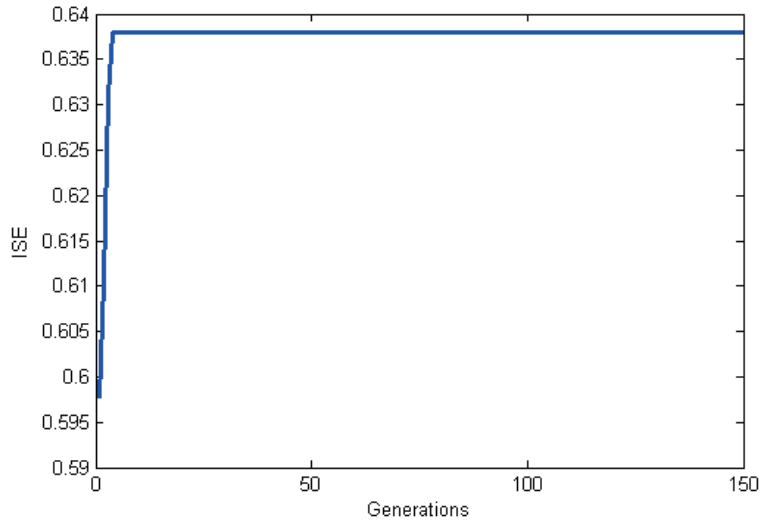

Fig. 10. (Color online) Inverse of minimum ISE of each generation.

As discussed, the pre-filter K_1 must also be calculated to meet the desired time domain response. The minimum ISE is applied to compare the step response to that of T_{ref}. The GA is applied to find the optimal parameter of K_1, which has the transfer function as shown in Eq. (30). The fitness function (the inverse of minimum ISE) is obtained as 0.638 in the 4th generation as shown in Fig. 10, whereas the step response is as shown in Fig. 11.

$$K_1(p_1) = \frac{1}{1.794 \times 10^{-4} s + 1} \tag{30}$$

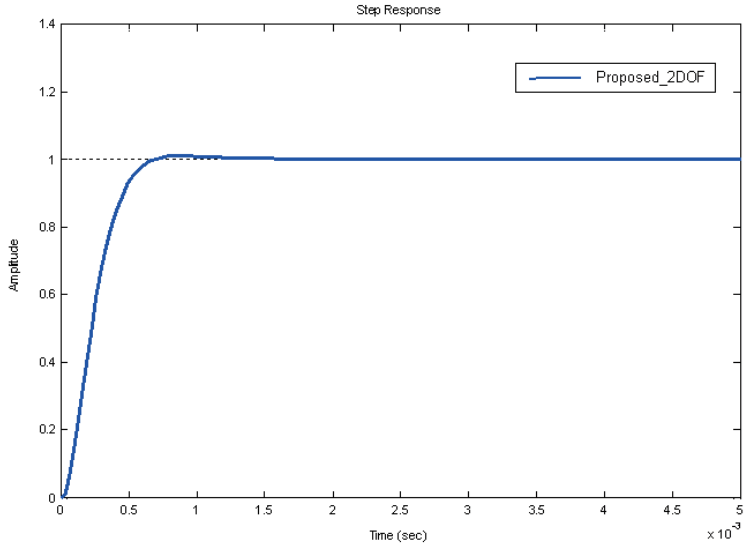

Fig. 11. (Color online) Step response of proposed technique by using 2DOF H_∞ loop shaping control.

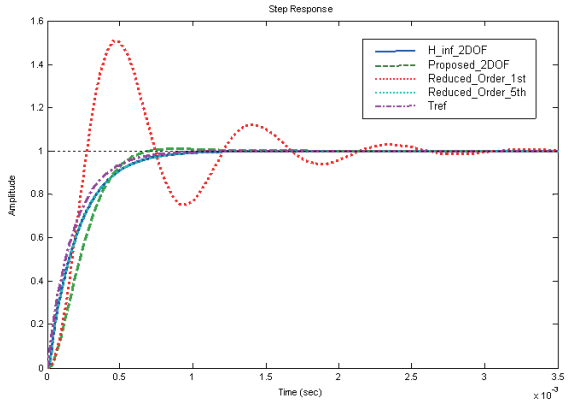

Fig. 12. (Color online) Step responses of each technique.

Four robust filters K_1 and controllers K_2 synthesized by different methods, such as the conventional 2DOF H_∞ loop shaping control, the proposed technique, and Hankel reduction model (1st and 5th orders), were applied to the ACMC buck converter voltage control system. The voltage step response and that of T_{ref} are simulated and plotted as depicted in Fig. 12. The performance indices are shown in Table 2.

As shown in Table 2, the ε of the system with K_1 and K_2 synthesized by the conventional 2DOF H_∞ loop shaping control and the 5th-order Hankel reduction model is 0.558, whereas that synthesized by the proposed technique is 0.594. Besides, the ε from the system with K_1 and K_2 synthesized using the 1st-order Hankel reduction model is only 0.151, although the orders of K_1 and K_2 are just one.

In the case of the rise time, settling time, and overshoot, only the results from the system with K_1 and K_2 synthesized using the 1st-order Hankel reduction model are the worst. As can be seen in Fig. 12, the overshoot and damped oscillation are significant, although the rise time is shorter.

Table 2
Comparison results of each controller and T_{ref}.

	Step response results			
	Rise time (ms)	Settling time (ms)	Overshoot (%)	Stability margin (ε)
H_inf_2DOF	0.446	0.814	0	0.558
Proposed_2DOF	0.383	0.605	0.97	0.594
Reduced_Order_1st	0.177	2.480	50.8	0.151
Reduced_Order_5th	0.446	0.814	0	0.558
T_{ref}	0.396	0.704	0	—

To further verify the robustness and performance of each controller, the parameters of the converter are adjusted to create the perturbed plant. These are classified into four different cases as follows: Case I: $R = 0.8\ \Omega$, $C = 220$ uF, Case II: $R = 1.5\ \Omega$, $C = 100$ uF, Case III: $R = 0.8\ \Omega$, $C = 100$ uF, and Case IV: $R = 1\ \Omega$, $C = 470$ uF.

The step responses of each perturbed plant controlled by each controller are plotted and shown in Fig. 13. The main performance indices of the perturbed plants are shown in Tables 3–6.

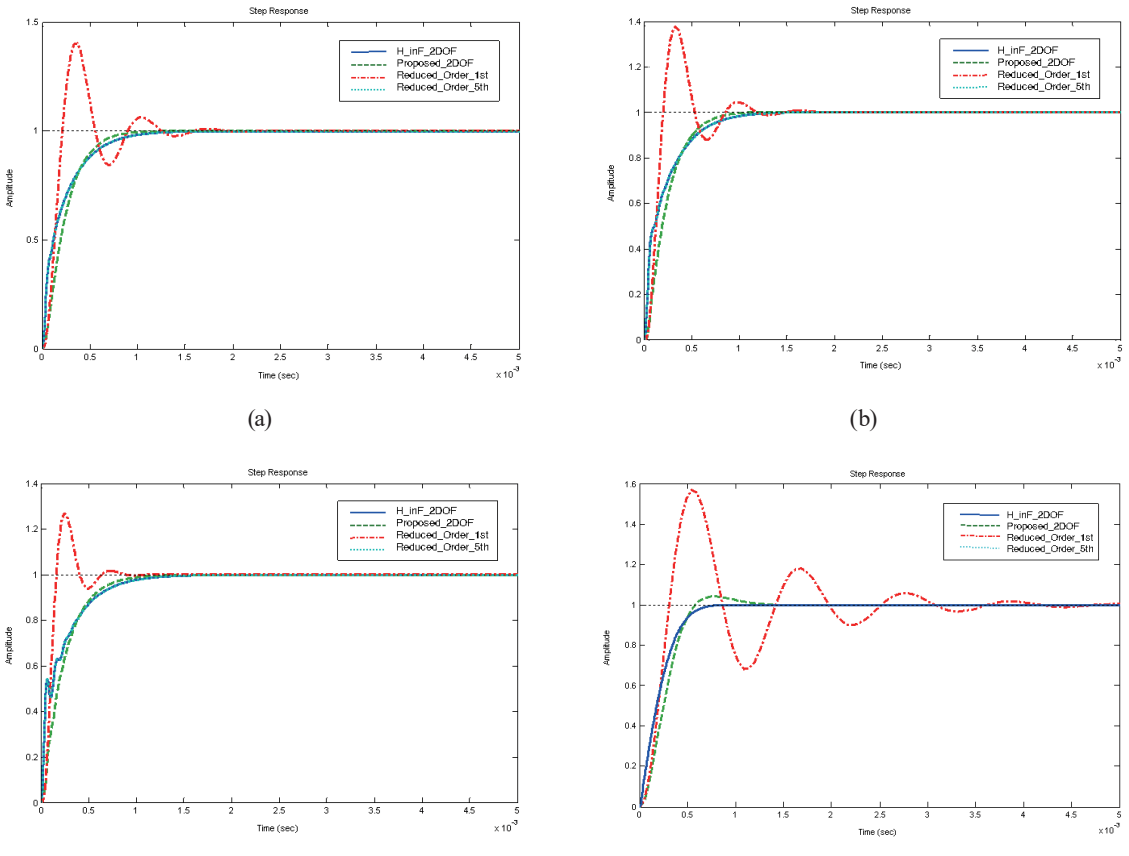

Fig. 13. (Color online) Simulation results showing the step responses of the perturbed plants. (a) Case I: $R = 0.8\ \Omega$, $C = 220$ uF, (b) Case II: $R = 1.5\ \Omega$, $C = 100$ uF, (c) Case III: $R = 0.8\ \Omega$, $C = 100$ uF, and (d) Case IV: $R = 1\ \Omega$, $C = 470$ uF.

Table 3
Comparison results of each controller in Case I.

	Step response results		
	Rise time (ms)	Settling time (ms)	Overshoot (%)
H_inf_2DOF	0.520	0.977	0
Proposed_2DOF	0.437	0.787	0.017
Reduced_Order_1st	0.136	1.450	40.3
Reduced_Order_5th	0.520	0.977	0.9770

Table 4
Comparison results of each controller in Case II.

	Step response results		
	Rise time (ms)	Settling time (ms)	Overshoot (%)
H_inf_2DOF	0.525	0.977	0
Proposed_2DOF	0.446	0.794	0
Reduced_Order_1st	0.124	1.100	37.5
Reduced_Order_5th	0.525	0.977	0

Table 5
Comparison results of each controller in Case III.

	Step response results		
	Rise time (ms)	Settling time (ms)	Overshoot (%)
H_inf_2DOF	0.557	1.040	0
Proposed_2DOF	0.483	0.880	0
Reduced_Order_1st	0.097	0.597	26.6
Reduced_Order_5th	0.557	1.040	0

Table 6
Comparison results of each controller in Case IV.

	Step response results		
	Rise time (ms)	Settling time (ms)	Overshoot (%)
H_inf_2DOF	0.407	0.626	0.09
Proposed_2DOF	0.372	1.050	4.22
Reduced_Order_1st	0.372	3.480	56.9
Reduced_Order_5th	0.407	0.626	0.09

The simulation results show that the step responses of the system with K_1 and K_2 synthesized by the proposed technique are close to the step responses of those synthesized by other techniques. A slightly low overshoot at 4.22% is exposed in case IV. However, the K_1 and K_2 synthesized by the proposed technique are only the 1st-order transfer functions. They can be implemented in real systems.

Furthermore, the K_1 and K_2 synthesized using the 1st-order Hankel reduction model are also the 1st-order transfer functions, but they cannot retain robustness and performance as their ε is only 0.151 ($\varepsilon < 0.25$).

The experiment was performed to substantiate the simulation results. The system having parameters shown in Table 1 controlled by K_1 and K_2 shown in Eqs. (29) and (30) is implemented. The implement system of the buck converter is shown in Fig. 14. The step response voltage of the

nominal ACMC buck converter plant is shown in Fig. 15. As shown, the step responses have a short settling time, a low maximum overshoot, and a zero steady-state error as shown in the simulation results.

The step response voltage for the perturbed plant, as shown in Fig. 16, also substantiates the simulation results. The slightly low overshoot also appears in the experimental results of case IV.

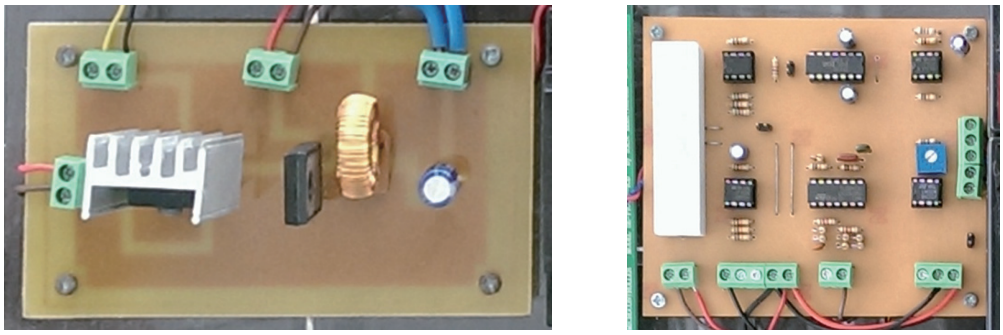

(a) (b)

Fig. 14. (Color online) Experimental circuit of ACMC buck converter. (a) Buck converter. (b) Current loop and proposed controllers.

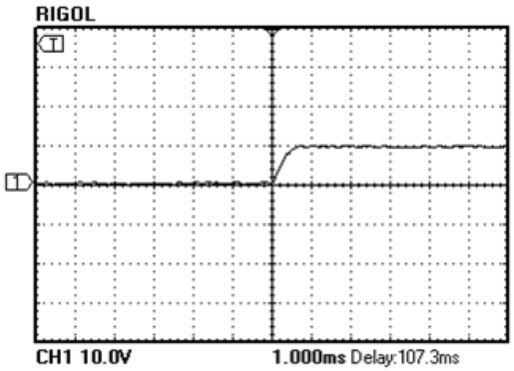

Fig.15. Experimental result showing voltage step response of nominal plant.

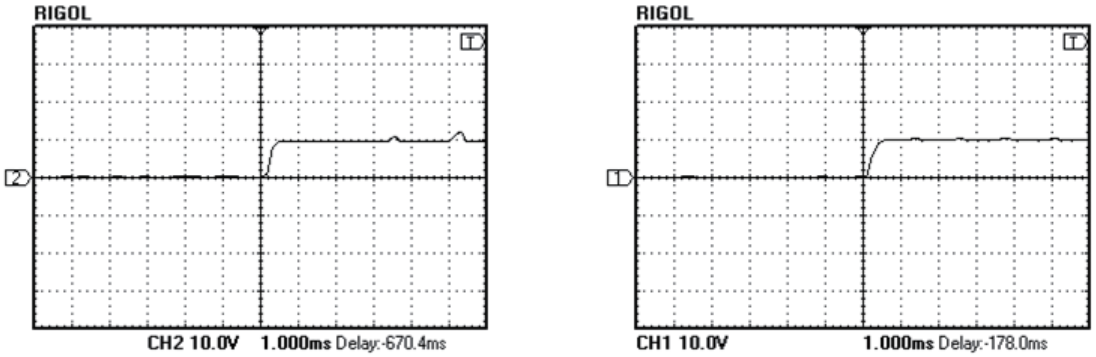

(a) (b)

Fig. 16. Experimental results showing step response voltage of perturbed plant in experiments. (a) Case I: R = 0.8 Ω, C = 220 uF, (b) Case II: R = 1.5 Ω, C = 100 uF.

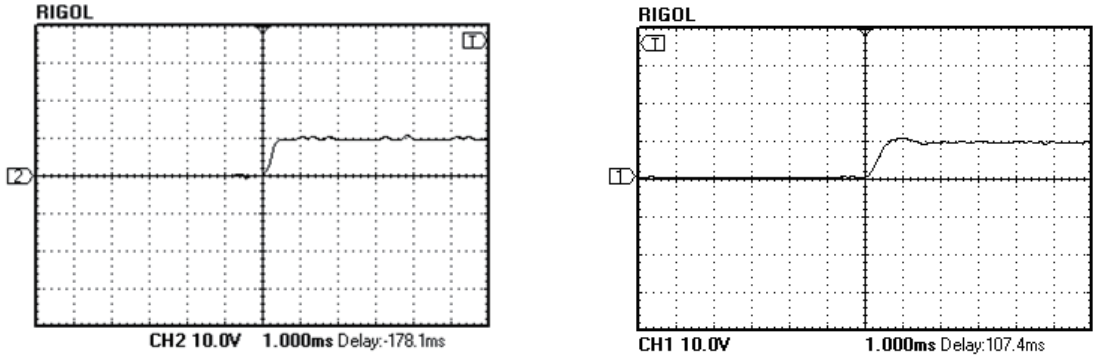

(c) (d)

Fig.16. (Continued) Experimental results showing step response voltage of perturbed plant in experiments. (c) Case III: $R = 0.8\ \Omega$, $C = 100$ uF and (d) Case IV: $R = 1\ \Omega$, $C = 470$ uF.

5. Conclusions

In this paper, we present the implementation of the voltage controller synthesized by the proposed technique called fixed structure 2DOF H_∞ loop shaping control using GA. The proposed technique helps reduce the order of the controller and filter synthesized by the conventional 2DOF H_∞ loop shaping method down to one, while retaining the robustness and high performance. The step response of the plant with the designed filter and controller is then compared among those of the plant with other designed filters and controllers, such as conventional 2DOF H_∞ loop shaping control and 1st-order and 5th-order Hankel reduction models. According to the simulation and experimental results, the proposed technique can be effectively applied to real systems, and the proposed technique will also be applicable to other systems.

Acknowledgments

This work was supported by the King Mongkut's Institute of Technology Ladkrabang Research Fund No. KREF045409. This work was also supported by the College of Data Storage Innovation.

References

1 S. Skogestad and I. Postlethwaite: Multivariable Feedback Control Analysis and Design (John Wiley & Sons, 2005) 2nd ed.
2 R. Miklosovic and Z. Gao: Ind. Appl. Soc. World **4** (2004). https://doi.org/10.1109/IAS.2004.1348669
3 J. F. Whidborne, I. Postlethwaite, and D.-W. Gu: IEEE Trans. Control Syst. Technol. **2** (1994) 455. https://doi.org/10.1109/87.338666
4 D. J. Hoyle, R. A. Hyde, and D,J.N. Limebeer: Proc. 1991 30th IEEE Conf. Decision and Control (IEEE, 1991) 1581–1585.
5 S. Kaitwanidvilai, P. Olranthichachat, and M. Parnichkun: Proc. 2008 Int. MultiConf. Engineers and Computer Scientists (IMECS, 2008). https://doi.org/10.1.1.148.7135
6 S. Kaitwanidvilai and M. Parnichkun: J. Rob. Mech. **16** (2004) 362. https://doi.org/10.20965/jrm.2004.p0362

7 N. Phurahong, S. Kaitwanidvilai, and A. Ngaopitakkul: Proc. 2012 Int. MultiConf. Engineers and Computer Scientists 2012. (IMECS 2012)
8 B. H. Cho, H. S. Bea, and J. H. Lee: Proc. 2009 IEEE 6th Power Electronics and Motion Control Conf. (IEEE, 2009) 202–210. https://doi.org/10.1109/IPEMC.2009.5289339
9 J. Sun and R. M. Bass: Proc. 1999 14th Annu. Applied Power Electronics Conf. and Exposition (APEC, 1999). https://doi.org/10.1109/APEC.1999.750488
10 W. Tang, F. C. Lee, and R. B. Ridley: IEEE Trans. Power Electron. **8** (1993) 112. https://doi.org/10.1109/63.223961
11 S. J. Young, Y. L. Jun, and J. Y. Myung: Proc. 1998 29th Annu. IEEE Power Electronics Specialists Conf. (IEEE, 1998) 1118–1124. https://doi.org/10.1109/PESC.1998.703144
12 J. Sebastian, P. J. Villegas, M. Hernando, F. Nuno, and F. Fernandez-Linera: IEEE Trans. Ind. Electron. **46** (1999) 569. https://doi.org/10.1109/41.767064
13 R. L. Lin, P. Y. Yeh, and C. H Liu: IEEE Trans. Power Electron. **27** (2012) 3186. https://doi.org/10.1109/TPEL.2011.2181999
14 I. Codreanu: Proc. 2007 Int. Semiconductor Conf. (2007). https://doi.org/10.1109/SMICND.2007.4519769
15 I. Saaki, P. C. Babu, X. K. Rao, and D. S. Prasad: Proc 2011 Power and Energy System (ICPS, 2011) 1–5. https://doi.org/10.1109/ICPES.2011.6156665